Nano Research

ISSN 1998-0124 CN 11-5974/O4
https://doi.org/10.26599/NR.2026.94908384

Research Article

Super-lubricating hydrogel enabled by microgel rolling and gradient porous structures

Song Yang[1,2], Chenxi Qin[2], Zhencai Xing[3], Ming Zhang[2](✉), Yanfei Ma[2](✉), Feng Zhou[2], Weimin Liu[1,2](✉)

[1] School of Materials Science and Engineering, Northwestern Polytechnical University, Xi'an 710072, China

[2] State Key Laboratory of Solid Lubrication, Lanzhou Institute of Chemical Physics, Chinese Academy of Sciences, Lanzhou 730000, China

[3] Shandong Laboratory of Yantai Advanced Materials and Green Manufacture, Yantai 264006, China

Nano Res., **Just Accepted Manuscript** • https://doi.org/10.26599/NR.2026.94908384

https://www.sciopen.com/journal/1998-0124 on Dec. 29, 2025

Just Accepted

TABLE OF CONTENTS (TOC)

Super-lubricating hydrogel enabled by microgel rolling and gradient porous structures

Song Yang[1,2], Chenxi Qin[2], Zhencai Xing[3], Ming Zhang[2]*, Yanfei Ma[2]*, Feng Zhou[2], and Weimin Liu[1,2]*

[1] School of Materials Science and Engineering, Northwestern Polytechnical University, Xi'an 710072, China

[2] State Key Laboratory of Solid Lubrication, Lanzhou Institute of Chemical Physics, Chinese Academy of Sciences, Lanzhou 730000, China

[3] Shandong Laboratory of Yantai Advanced Materials and Green Manufacture, Yantai 264006, China

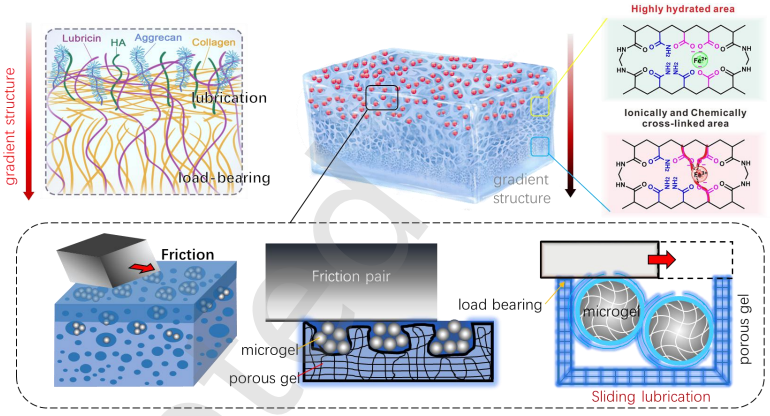

This manuscript demonstrates a conceptually novel strategy to construct robust lubricated soft material surfaces based on gradient structure for dissipating contact stress, microgel rolling for lubrication to simultaneously achieve high load-bearing (5 N) and super-lubrication (0.006).

Nano Research

ISSN 1998-0124 CN 11-5974/04
https://doi.org/10.26599/NR.2026.94908384

Research Article

Super-lubricating hydrogel enabled by microgel rolling and gradient porous structures

Song Yang[1, 2], Chenxi Qin[2], Zhencai Xing[3], Ming Zhang[2, *], Yanfei Ma[2, *], Feng Zhou[2], and Weimin Liu[1, 2, *]

[1] School of Materials Science and Engineering, Northwestern Polytechnical University, Xi'an 710072, China
[2] State Key Laboratory of Solid Lubrication, Lanzhou Institute of Chemical Physics, Chinese Academy of Sciences, Lanzhou 730000, China
[3] Shandong Laboratory of Yantai Advanced Materials and Green Manufacture, Yantai 264006, China

Received: 5 November 2025 / **Revised:** 28 December 2025 / **Accepted:** 29 December 2025

ABSTRACT

Hydrogels, with their tissue-like properties, biocompatibility, and soft properties, are potential biomimetic cartilage replacement materials. However, the conflict between their surface lubricity and load-bearing properties significantly limits their application. Here, we developed a structure-based hydrogel with super-lubricity and high load-bearing properties. Through UV-controlled dissociation, a gradient hydrogel surface was constructed. This structure effectively dissipates normal contact stress while maintaining a high surface hydration level, enhancing load-bearing capacity. Furthermore, micron-sized spherical gel particles were prepared using an emulsion method and incorporated into the highly hydrated polymer network, further enhancing the load-bearing capacity of the porous hydrogel and significantly reducing the coefficient of friction (COF) by converting sliding friction into rolling friction. Ultimately, through multiple synergistic effects, we achieved ultra-low friction performance, with a COF of approximately 0.0064 after 20,000 cycles under a 5 N load. This innovation provides an alternative solution for future biomimetic articular cartilage.

KEYWORDS

gradient hydrogel, micron particles, high-load bearing, low friction

1 Introduction

Human articular cartilage [1-6] features a combination of high load-bearing capacity and low friction, yet replicating these properties with synthetic materials remains a challenge. Since natural cartilage cannot regenerate, the issue becomes more urgent as the population ages, leading to an increase in joint diseases caused by cartilage deterioration. These conditions often result in significant pain and disability [7-9]. Currently, the primary treatment for severe cases is joint replacement surgery, typically using titanium alloys [10-12]. While titanium alloys are favored in orthopedics for their biocompatibility and lightweight nature, their lubrication and wear resistance are inadequate. Consequently, improving the performance of artificial joint materials remains a critical area of research.

Hydrogels, with their high water content, excellent biocompatibility, and tissue-like qualities, are promising candidates for artificial joint cartilage. However, their inherently fragile mechanical properties limit their applicability, particularly under high loads, which can result in potential surface damage and lubrication failure. Research indicates that increasing the hydrogel's modulus can improve its load-bearing capacity [13-15], but this often results in a loss of water content and surface lubricity [16-18]. Conversely, hydrogels with lower modulus and higher hydration can achieve super-lubricity, but at the cost of reduced mechanical strength [19-22]. Achieving a balance between high load-bearing ability and low friction remains a major challenge [23-25]. Developing hydrogel materials that effectively combine both properties is a key focus of ongoing research in the field.

Joints in the human body that experience substantial friction and impact, such as the knee, hip, and shoulder, are synovial joints. Articular cartilage, acting as the "cushion" at the ends of bones, serves as the primary surface for lubrication. Its effectiveness is due to its unique gradient structure, extending from the surface to the deeper layers, which is essential for both lubrication and load-bearing functions [26-28]. Inspired by articular cartilage, we designed a structural super-lubricious hydrogel (SLH) featuring a gradient porosity along its length, with a transition from high to low water content and modulus. This gradient structure is constructed by UV-controlled dissociation. Using vertical UV light irradiation, the surface of the hydrogel receives the highest light intensity. As the UV penetrates the hydrogel, scattering and refraction cause the intensity to decrease gradually with depth. This creates a gradient in the hydrogel's properties, effectively reducing friction while enhancing load-bearing capacity. Additionally, spherical microgel particles are embedded within the high water-content polymer network on the surface. These micron particles convert sliding friction into rolling friction, further reducing resistance. Combined with the load support provided by the gradient structure, this design achieves a balance between high load-bearing ability and low friction. Collectively, these structural features endow the hydrogel with excellent fatigue resistance, high load capacity, and an ultra-low coefficient of friction (approximately 0.006 after 20,000 cycles under 5 N), which makes it a promising candidate for next-generation cartilage repair and artificial joint applications.

Address correspondence to Ming Zhang, zhm@licp.cas.cn; Yanfei Ma, mayanfei@licp.cas.cn; Weimin Liu, wmliu@licp.cas.cn

2 Experimental section

2.1 Materials

2-hydroxy-4'-(2-hydroxy-ethoxy)-2-methylphenylacetone (2959), N, N'-methylenediacrylamide (MBAA), Acrylic acid (AAc), acrylamide (AAm), were from J&K Chemical Co., Ltd. Cinnamyl alcohol polyoxyethylene ether (Brij 30) and sodium diisooctyl succinate sulfonate (AOT) were derived from Aladdin. Cyclohexane, anhydrous ethanol, ammonium persulfate (APS), and hexahydrate ferric chloride were from China National Pharmaceutical Group Chemical Reagent Co., Ltd.

2.2 p(AAc-co-AAm) hydrogel preparation

Pour acrylamide (AAm, 6.397 g), acrylic acid (AAc, 2 g), crosslinking agent N, N'-methylenediacrylamide (MBAA, 0.012 g), initiator 2-hydroxy-4'-(2-hydroxy-ethoxy)-2-methylphenylacetone (2959, 0.06 g), and deionized water (30 g) into a beaker and stir until fully dissolved. Vacuum the solution for 30 minutes to remove dissolved gases from the solution. Pour the solution into a glass mold (1 mm thick) and irradiate the solution with a low power ultraviolet lamp (365 nm, 2.0 mW/cm^2) for 4 hours to obtain hydrogel. Soak the hydrogel in $FeCl_3$ solution (0.3 mol/L) for 3 days to obtain p(AAc-*co*-AAm)-Fe^{3+} hydrogel, and store it in deionized water for standby. Soak p(AAc-*co*-AAm)-Fe^{3+} hydrogel in deionized water again, and irradiate it for 2 hours, 3 hours, and 5 hours with high power ultraviolet lamp (365 nm, 160 mW/cm^2), becoming gradient hydrogel with different light intensity.

2.3 p(AAc-co-AAm) micron particles preparation

Micron particles are prepared by reverse emulsification method. Firstly, prepare a reverse emulsion by pouring two surfactants, namely thymol polyoxyethylene ether (Brij 30, 4.34 g), sodium diisooctyl succinate sulfonate (AOT, 8.67 g), and cyclohexane (81 g), into a beaker and stirring thoroughly to prepare the reverse emulsion. Then prepare an aqueous solution by pouring acrylic acid (AAc, 0.3815 g), acrylamide (AAm, 0.3206 g), crosslinking agent N, N'-methylenediacrylamide (MBAA, 0.12 g), initiator ammonium persulfate (APS, 0.318 g), and deionized water (4.86 g) into a beaker and stirring thoroughly to prepare the aqueous solution. Pour the reverse emulsion and half of the aqueous solution into a three necked flask, protect under N_2 atmosphere, and stir mechanically (1200 rpm). After 30 minutes, heat to 60 °C and hold for 2 hours. Blow the remaining half of the aqueous solution with N_2 for 30 minutes, pour it into a three necked flask, and continue heating and stirring for 2 hours. Stop heating and mechanical stirring, and wait for the solution in the three necked flask to cool naturally before stopping the N_2 atmosphere protection. Solid micron particles were observed at the bottom of the flask. Most of the cyclohexane and surfactants were removed by rotary evaporation (at a temperature of 40 °C), and 100 g of anhydrous ethanol was added to prepare a suspension of the micron particles. Centrifuge the suspension with a centrifuge (3200 rcf) for 10 minutes to remove the supernatant, rinse and wash with deionized water, and repeat this process 3 times. Pour the micron particle suspension into a dialysis bag (10 kDa) and dialyze for 3 days, changing the water every 12 hours. The prepared suspension of micron particles should be stored in deionized water, shaken well before use, and then dropped on the surface of the hydrogel, standing for 10 minutes, so that the micron particles sink into the pores of the hydrogel.

2.4 Ultraviolet irradiation

Use a commercial UV lamp with an intensity of 2.0 mW/cm^2 and 160 mW/cm^2 for long wave UV (365 nm) irradiation (measured using an LS125 UV photometer calibrated at 365 nm).

2.5 Scanning electron microscope

The sample used for SEM testing was frozen in liquid nitrogen for 10 minutes using a scanning electron microscope (SEM, ZEISS Sigma 360, Germany), and then dried for 48 hours using freeze-drying at -40 °C and 1 Pa.

2.6 Transmission electron microscope

Transmission electron microscopy (TEM, JEOL JEM-F200, Japan) was used for micron particle morphology characterization. The sample should be dropped onto a copper mesh.

2.7 Atomic force microscopy

Atomic force microscopy (AFM, Bruke MultiMode 8) is used for characterizing the morphology of micron particles.

2.8 X-ray photoelectron spectroscopy (XPS) analysis

The surface elements of the hydrogel film were analyzed by X-ray photoelectron spectroscopy (Thermo Scientific K-Alpha). The sample was frozen in liquid nitrogen for 10 minutes, and then dried using freeze-drying at -40 °C and 1 Pa for 48 hours. Scanning C and Fe elements, the content ratios of different ions Fe^{3+}/Fe^{2+} on the sample surface were obtained based on the peak positions and shapes of the spectra.

2.9 Tensile and compressive strength tests

The test was conducted using an electronic universal testing machine (EZ-test, Shimadzu, Japan) equipped with a 500 N force sensor. Fix the sample using standard fixtures.

2.10 Friction test

Record the friction coefficient under different loads at 25 °C on a traditional CSM friction meter. The lubricant is deionized water. Use a stainless-steel column with a diameter of 5 mm as the sliding pair. The sliding distance is 10 mm.

3 Results and discussion

3.1 Design and preparation of structural super-lubricious hydrogel (SLH)

Inspired by the complex structure of cartilage tissue (Fig.1A), we developed a structural super-lubricious hydrogel (SLH). The hydrogel material has a porous structure that decreases gradually from top to bottom in the longitudinal direction, and the modulus and hydration degree also decrease accordingly. This structure was primarily achieved through UV light, which reduces the trivalent iron in the hydrogel to divalent iron, reducing the hydrogel's crosslink density. Furthermore, due to the loss of light energy from the top down, a gradient porosity

was generated from top to bottom. On the surface of the hydrogel, spherical microgels based on emulsion polymerization were embedded in the polymer network with low crosslinking and high hydration caused by photodissociation, which converts surface sliding into rolling friction, further reducing the interfacial friction coefficient, and at the same time reducing the stretching and fracture of low modulus molecular segments during sliding friction. Detailed, the precursors of hydrogel were synthesized by light-initiated free radical polymerization.

Acrylamide (AAm), acrylic acid (AAc), the crosslinker N, N'-methylenebisacrylamide (MBAA), and the photoinitiator 2-hydroxy-4'-(2-hydroxyethoxy)-2-methylpropiophenone (2959, 0.06 g) were dissolved in an appropriate amount of deionized water and then irradiated with 365 nm UV light for 4 hours to prepare the p(AAc-*co*-AAm) hydrogel. Furthermore, the p(AAc-*co*-AAm) hydrogel was immersed in a 0.3 mol/L $FeCl_3$ solution to undergo double crosslinking (carboxylic acid coordinated with iron) to form the p(AAc-*co*-AAm)-Fe^{3+} hydrogel. The gradient hydrogel was prepared by reducing ferric iron to ferrous iron via UV light, thereby reducing the crosslink density. Specifically, gradient hydrogels were prepared according to different UV irradiation time based on the p(AAc-*co*-AAm)-Fe^{3+} hydrogel was exposed to 365 nm ultraviolet light (Fig. 1B). After UV irradiation, the hydrogel exhibits a gradient in the normal direction, with a loose, porous surface structure that decreases in pore size and increases in density from top to bottom.

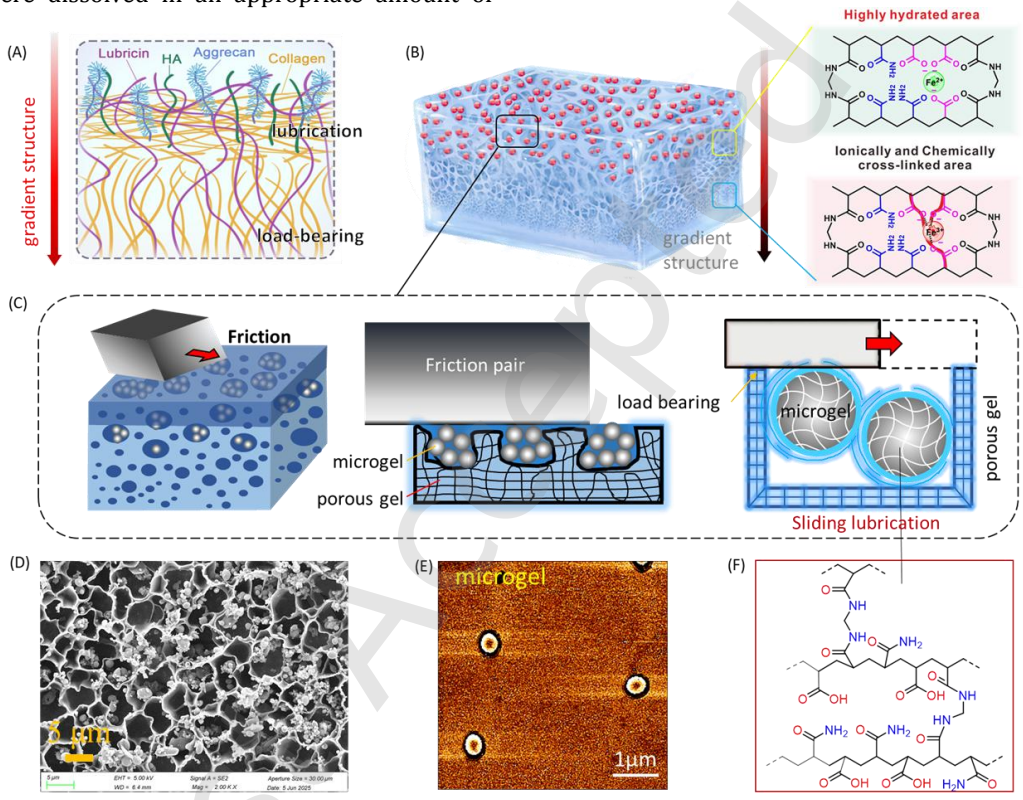

Fig. 1 Design principle of structural super-lubricious hydrogel (SLH). (**A**) Structure diagram of gradient hydrogel. (**B**) Schematic diagram of the mechanism of gradient hydrogel composition, embedded micron particles and UV light leading to the hydrogel surface from compact to loose. (**C**) Schematic diagram of micron particle wear reduction mechanism. (**D**) SEM images of gradient hydrogels and micron particles. (**E**) AFM images of micron particles. (**F**) The polymer structure of micron particles.

In order to further improve the lubricity of gradient hydrogel, we introduced micro gel into the highly hydrated hydrogel surface and embedded it in the pores of the hydrogel. As shown in Fig. 1C, the micro-particles appeared to be spherical. When the gradient hydrogel with microgels was rubbed against the surface of other media, the sliding friction was converted into rolling friction, which greatly reduced the friction coefficient. As shown in the scanning electron microscope (SEM) in Fig. 1D, the micron particles were embedded in the pores of gradient hydrogel. Because the hardness of p(AAc-*co*-AAm) micron particles was hard, the wear of gradient hydrogel can also be reduced in the friction mode. We characterized the morphology of the micron particles using atomic force microscopy (AFM) [29-33] (as shown in Fig. 1E) and found that the size of the micron particles was nearly spherical with a diameter of approximately 0.4 μm. The preparation method of the micron particles mainly adopts an emulsion method, the detailed preparation steps are shown in the experimental section (Fig. 1F).

3.2 Construction and mechanical properties of the gradient hydrogel

Exposure to high-energy ultraviolet light causes Fe^{3+} ions to reduce to Fe^{2+}. This change in oxidation state alters the affinity between the iron ions and AAc groups, which can lead to the formation of pores on the hydrogel surface. To verify this, we examined whether the element composition and surface morphology of the gradient hydrogel change under UV irradiation. We conducted in-depth research on the effect of UV induced dissociation, with a particular focus on the conversion of Fe^{3+} to Fe^{2+}, as shown in Fig. 2A. This process influences the surface properties of the hydrogel and plays a critical role in its

structural evolution. We employed X-ray photoelectron spectroscopy (XPS) [34–38] to analyze changes in the surface element composition of the hydrogel before and after UV irradiation. We compared samples irradiated for 1 hour and 5 hours (Fig. 2B, C). In the XPS spectra, there are two major characteristic peaks and two smaller ones for Fe^{3+} and Fe^{2+}. We focused on the peaks with larger areas for analysis. Results showed that, after UV exposure, the area corresponding to Fe^{3+} decreased while the Fe^{2+} area increased with longer UV exposure, indicating that Fe^{3+} was progressively reduced to Fe^{2+} under UV irradiation.

We examined the sample using a scanning electron microscope (SEM) to more intuitively display the gradient structure. We selected images of the surface and cross-section that were not exposed to UV light, as well as those illuminated for 2 hours and 5 hours. The resulted revealed that the surface (Fig. 2D) and cross-section (Fig. 2E) of the p(AAc-*co*-AAm)-Fe^{3+} hydrogel without UV exposure appeared densely packed and uniform. In contrast, the surfaces exposed to UV light for 2 hours (Fig. 2F) and 5 hours (Fig. 2H) displayed increasingly porous structures, with pore sizes expanding as exposure time lengthened. This occurs because UV light converts Fe^{3+} into Fe^{2+}, disrupting the original coordination bonds between Fe^{3+} and the carboxyl groups. As a result, the stable hydrogel network gradually collapses and shrinks into pores over time. Similarly, the cross-sections of samples exposed to UV light for 2 hours (Fig. 2G) and 5 hours (Fig. 2I) showed a clear two-layer structure. The upper layer was loose and porous, while the lower layer remained dense. This layered morphology visually demonstrates the transformation of Fe^{3+} into Fe^{2+} within the hydrogel during UV irradiatio

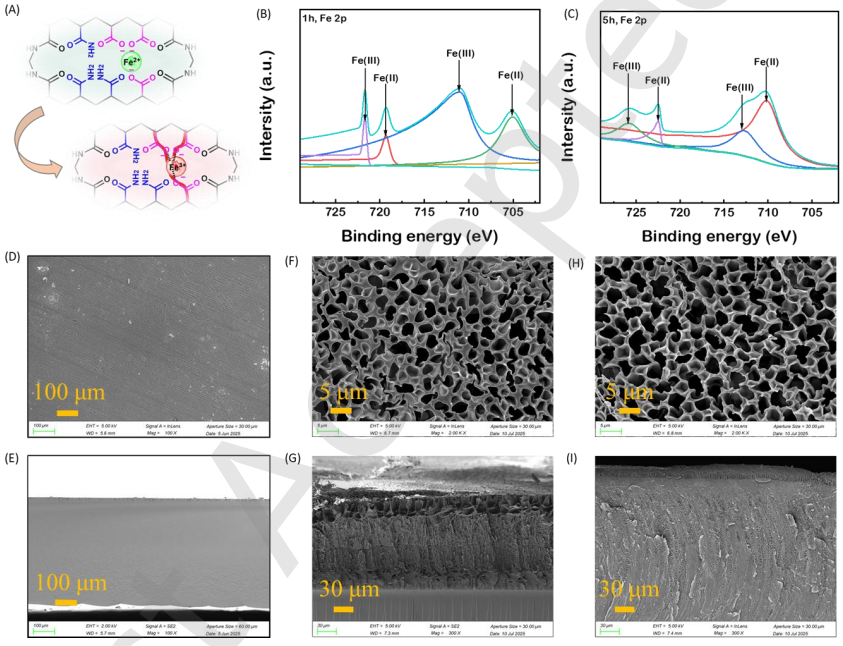

Fig. 2 Surface structure and element content of the gradient hydrogel. (**A**) The gradient hydrogel converts Fe^{3+} into Fe^{2+} under UV irradiation. (**B, C**) XPS testing under UV irradiation for 1 hour and 5 hours. (**D, E**) SEM images of gradient hydrogels with dense surface and cross section structure in the absence of light. (**F, G**) SEM images of pores and cross section delamination appeared on the surface of gradient hydrogels exposed to UV light for 2 hours. (**H, I**) The surface pores of gradient hydrogels exposed to UV light for 5 hours become larger and the cross section was divided into thickened SEM images.

Since UV-induced dissociation causes pore formation in the originally compact hydrogel, which could compromise its mechanical properties, it was important to evaluate the mechanical performance of the gradient hydrogels. Generally, as UV exposure time increases, the tensile and compressive strength, as well as the modulus, tend to decline. In our experiments, we measured the tensile strength and modulus of the gradient hydrogel after UV irradiation for 2 hours, 3 hours, and 5 hours, as well as without UV exposure (Fig. 3A, B). The resulted consistently showed that both tensile strength and modulus decreased with longer UV exposure, indicating a decline in mechanical integrity as dissociation progresses. Specifically, the tensile strength decreased with increased UV exposure: it was 16.780 MPa at 0 hours, 13.806 MPa at 2 hours, 12.398 MPa at 3 hours, and 11.510 MPa at 5 hours. In contrast, the strain at break increased sharply, reaching 109.8 % at 0 hours, 135.2 % at 2 hours, 144.2 % at 3 hours and 172.5 % at 5 hours. These observations indicate that UV irradiation causes the hydrogel surface to soften rapidly. Correspondingly, the elastic modulus also decreased progressively, from 53.629 MPa at 0 hours, 46.549 MPa at 2 hours, 41.509 MPa at 3 hours and 35.921 MPa at 5 hours. In addition, we measured their compressive strength and modulus (Fig. 3C, D). The compressive strength decreased with increasing UV exposure time, from 1.456 MPa at 0 hours, 1.100 MPa at 2 hours, 0.808 MPa at 3 hours and 0.731 MPa at 5 hours. Similarly, the compressive modulus declined from 29.955 MPa at 0 hours, 22.697 MPa at 2 hours, 16.096 MPa at 3 hours and 13.990 MPa at 5 hours. In the compression tests, a 5 % strain was applied, resulting in lower values compared to the tensile strength tests.

Nano Research
ISSN 1998-0124 CN 11-5974/04
https://doi.org/10.26599/NR.2026.94908384

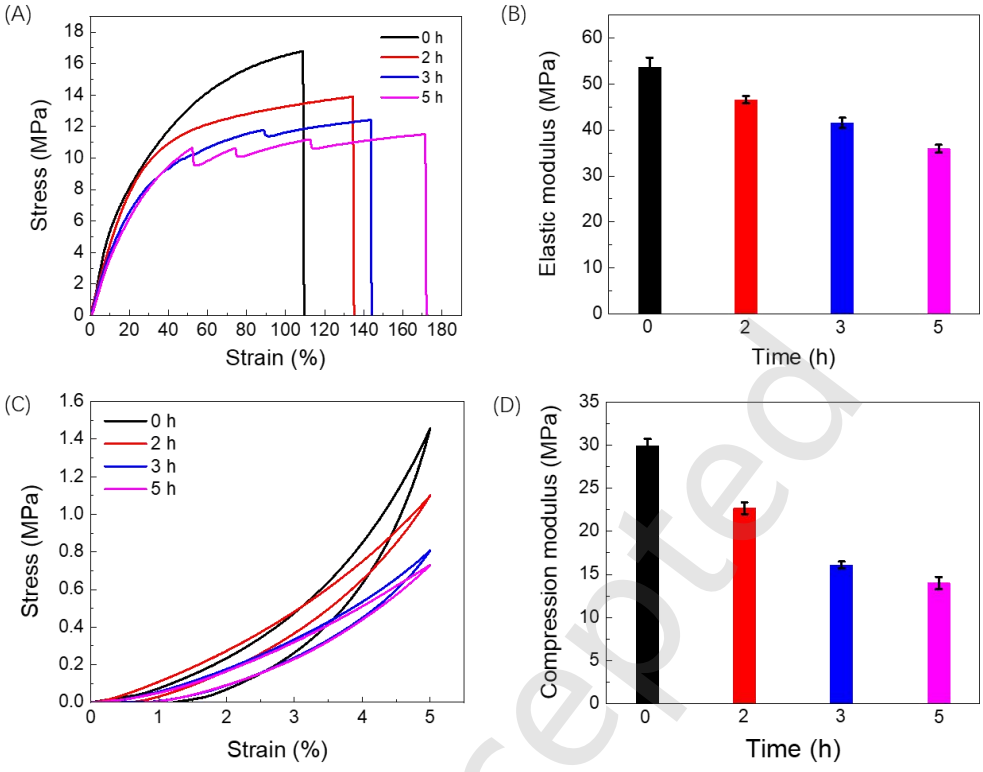

Fig. 3 Mechanical properties of the gradient hydrogel. (**A**) The tensile stress-strain curve and (**B**) elastic modulus of the hydrogel after 0 hours, 2 hours, 3 hours and 5 hours of UV irradiation. (**C**) Compressibility and (**D**) compression modulus of the hydrogel after 0 hours, 2 hours, 3 hours and 5 hours of UV irradiation.

We also examined how incorporating p(AAc-*co*-AAm) micron particles affected the mechanical properties of gradient hydrogels. Compared to hydrogels without micron particles, those containing micron particles showed a higher modulus, which influenced their strain capacity and strength. Since the hydrogel without UV exposure remains relatively dense and does not incorporate micron particles, our analysis focused on hydrogels subjected to 2, 3, and 5 hours of UV irradiation. Specifically, the tensile strength and strain (Fig. S1) were measured at 9.638 MPa / 82.4 %, 9.050 MPa / 89.1 % and 7.541 MPa / 105.5 %, respectively. The tensile modulus (Fig. S2) decreased from 49.192 MPa at 2 hours, 42.976 MPa at 3 hours and 38.326 MPa at 5 hours. Similarly, the compressive strength and modulus (Fig. S3, S4) were 1.262 MPa / 49.193 MPa, 0.977 MPa / 42.976 MPa and 0.884 MPa / 38.326 MPa for the respective irradiation times. Overall, the results were consistent between tensile and compressive tests. Embedding micron particles led to a reduction in strain capacity and strength but resulted in an overall increase in the modulus. This indicates that while the micron particles enhance stiffness, they slightly reduce the material's deformability.

3.3 Structure and stress distribution of SLH

We used transmission electron microscopy (TEM) to analyze the morphology of p(AAc-*co*-AAm) micron particles, as shown in Fig. 4A. The micron particles had an approximate diameter of 0.4 μm. Atomic force microscopy (AFM) testing showed that their surface adhesion force was about 310 pN (Fig. 4B), which was one order of magnitude smaller than the surface adhesion force of normal materials, suggesting that our fine particles had a super lubricating effect [29-33]. Scanning electron microscopy (SEM) images of micron particles mounted on a gradient hydrogel surface showed that they remained encapsulated within the hydrogel matrix (Fig. 4C). Fig. 4D and 4E display SEM images of the SLH surface of non-doped and doped micron particles, respectively. The gradient structure and micron particle integration of SLH may affect the interfacial contact stress, so we simulated the interfacial contact stress through COMSOL. Because the modulus of the p(AAc-*co*-AAm) micron particles is higher than that of the surface lubrication layer, mechanical simulations illustrate how these particles effectively distribute the applied load downward (Fig. 4F). Their near-spherical morphology enables them to support high loads and convert sliding friction into rolling friction, which reduces the overall friction coefficient of the hydrogel. This design integrates micron particles within the hydrogel to achieve high load-bearing capacity and low friction at the microscopic level. Simultaneously, the gradient structure gradually transitions from the top lubrication layer to the dense, load-bearing core at the macroscale. Simulation analysis confirmed that this soft-to-hard contact structure (Fig. 4G) disperses stress more effectively than a uniform hard contact structure (Fig. 4H). This configuration was expected to notably improve the wear resistance of the hydrogel, enhancing its durability in practical applications. In conclusion, mechanical analysis shows that, compared to a single hard hydrogel, the

soft elastomer layer in the double hydrogel reduces stress concentration and dissipates stress more effectively, thereby enhancing load-bearing capacity. The addition of spherical micron particles to the soft elastomer layer shifts the friction mode from sliding to rolling, which not only further improves lubrication but also increases the overall load-bearing capacity of the hydrogel.

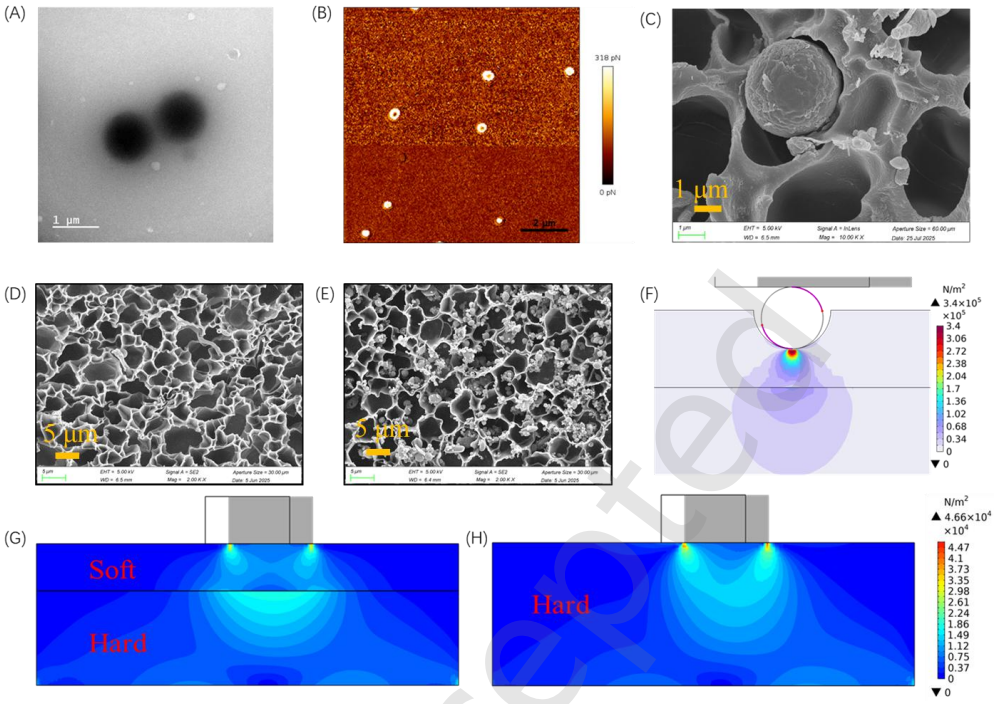

Fig. 4 Surface structure and mechanical simulation of SLH. (**A**) TEM image of micron particles with a diameter of approximately 0.4 μm. (**B**) The adhesion force of the micron particles measured by AFM image is approximately 310 pN. (**C**) SEM images of micron particle embedded gradient hydrogel. (**D, E**) SEM image of gradient hydrogel with or without incorporation of micron particles under UV light for 2 hours. (**F**) Comsol software was used to simulate the stress analysis of the contact point between micron particles and hydrogel. (**G, H**) Comsol software was used to simulate and analyze the stress analysis of soft-hard and hard- hard hydrogels.

3.4 Friction and wear resistance

We conducted frictional behavior studies using a Friction and Wear Tester (CSM) to understand the high load-bearing and low friction performance of SLH. The friction pair consisted of a circular steel column with a 5 mm diameter, with deionized water acting as the lubricant, and was subjected to face-to-face reciprocating friction. Initially, we measured the coefficient of friction (COF) of the control hydrogel under various loads without UV light and micron particles. As shown in Fig. S5, the COF increased with higher loads, starting at approximately 0.065 at 1 N and reaching up to 0.30 at 20 N. The gradient surface structure effectively reduced surface friction. After 2 hours of UV irradiation, the COF dropped to one-tenth of its original value. Interestingly, as the load increased, the COF first decreased, reaching a minimum of about 0.016 at a 3 N load, before it started to increase again (Fig. 5A). As the irradiation time extended to 3 hours, more trivalent iron was reduced to divalent iron, resulting in a looser surface polymer network with higher water content. However, this excessive looseness significantly increases the material's deformation resistance, impacting interfacial tribological behavior. As shown in Fig. S6, the COF initially decreases and then rises with increasing load, reaching a minimum value of approximately 0.038 at a 3 N load. Overall, the tribological performance after 2 hours of UV irradiation was superior to that observed after 3 hours.

Transitioning the hydrogel surface's friction mode from sliding to rolling effectively enhances its lubricity. We embedded p(AAc-*co*-AAm) microgel particles within the hydrogel's porous structure, enabling rolling lubrication within a confined space (Fig. 5B). With the introduction of micron particles, the COF's minimum value was observed at a 5 N load, owing to the improved load-bearing capacity. As the micron particles transitioned the friction from sliding to rolling, the COF was reduced to 0.0083, achieving super-lubrication. Subsequently, we conducted long-term friction tests at a 5 N load over 20,000 reciprocating cycles. As illustrated in Fig. 5C, the COF gradually decreased with increased friction cycles, reaching a super-lubrication level of 0.0064. Additionally, the friction curve remained smooth before and after the tests, indicating minimal wear on the hydrogel—evidenced by the wear images—demonstrating that our p(AAc-*co*-AAm) micron particles significantly enhance the wear resistance of gradient hydrogels.

In summary, the high-water content and gradient structure of the SLH surface were fundamental to enhancing its durable lubrication. The embedded micron particles serve two key roles: first, they transform sliding friction into rolling friction, significantly reducing the friction coefficient; second, their high modulus increases the hydrogel's load-bearing capacity, helping to prevent collapse and improving wear resistance. In conclusion, these gradient hydrogels and micron particles demonstrated strong potential as materials for bio-inspired

articular cartilage, combining excellent lubricity with mechanical stability.

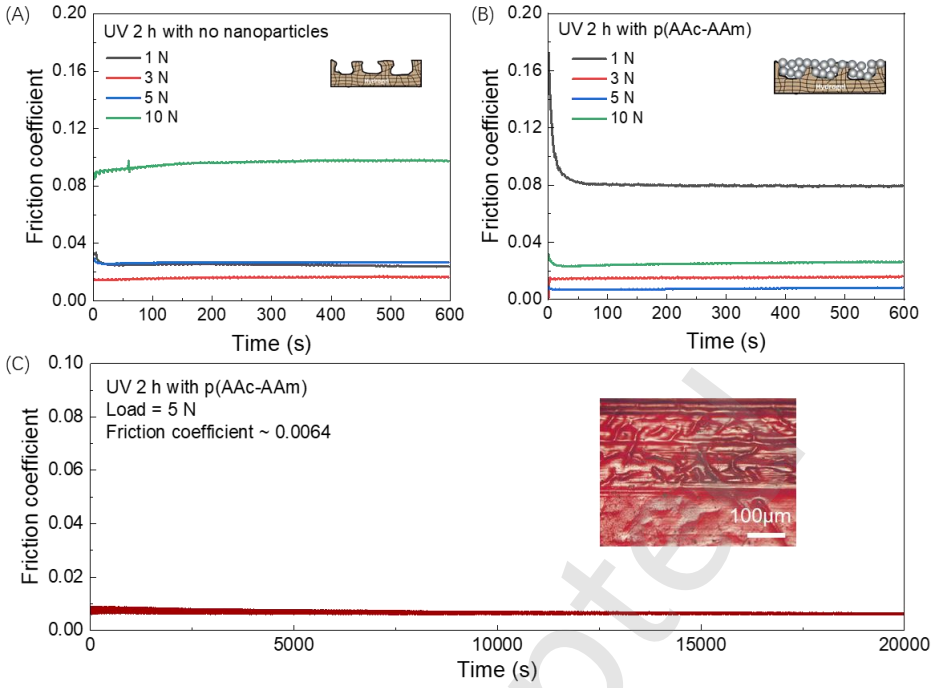

Fig. 5 Lubrication and wear resistance performance. (**A**) The friction coefficient under the condition of no micron particles added, 2 hours of UV irradiation, and a load of 3 N. (**B**) When adding micron particles, irradiating with ultraviolet light for 2 hours, and loading with 5 N, the friction coefficient was minimized. (**C**) Using gradient hydrogel with UV light for 2 hours, loading 5 N, adding micron particles, the friction curve of 20000 cycles, the lowest friction coefficient was about 0.0064.

4 Conclusions

In summary, to overcome the challenge of balancing high load-bearing capacity with low friction, a key issue in designing hydrogel-based artificial articular cartilage, we developed structural super-lubricating hydrogels. They feature a gradient structure along their longitudinal direction and a porous, highly hydrated surface. Embedded within this porous structure, cross-linked polymer microgels create a confined environment that facilitates rolling motion, thereby enhancing lubrication. Material Design encompasses two key innovative strategies. First, we employed photodissociation to create a gradient structure inspired by natural cartilage. This approach successfully achieved a balance of high load-bearing capacity and low friction, resulting in a hydrogel with a friction coefficient of 0.02 under a 5 N load, an order of magnitude lower than that of a non-gradient, high-modulus hydrogel under the same conditions. To further reduce surface friction, we embedded spherical microgels within a highly hydrated polymer network. This modification transformed sliding friction into rolling friction, effectively minimizing stress on surface polymer chains during movement. As a result, the hydrogel demonstrated enhanced durability and long-term lubrication performance. As a result, these strategies enabled the hydrogel to reach super-low friction and durable lubrication, with a friction coefficient of approximately 0.0064 under a 5 N load after 20,000 cycles. This work introduces a novel approach with potential for the development of biomimetic materials for joint repair and artificial cartilage, paving the way for future advancements in this field.

Acknowledgements

The authors gratefully acknowledge the financial support from key research project from the Key Program of the Chinese Academy of Sciences (RCJJ-145-24-42), Young Elite Scientists Sponsorship Program by CAST (2023QNRC001). The National Science Foundation of China (22575256), the Strategic Priority Research Program of the Chinese Academy of Sciences (XDB0470301).

Electronic Supplementary Material: Supplementary material (please give brief details, e.g., further details of the annealing and oxidation procedures, STM measurements, AFM imaging and Raman spectroscopy measurements) is available in the online version of this article at https://doi.org/10.26599/NR.2026.94908384.

References

[1] Wang, M.; Wu, Y.; Li, G.; Lin, Q.; Zhang, W.; Liu, H.; Su, J. Articular cartilage repair biomaterials: strategies and applications. *Mater. Today Bio* **2024**, *24*, 100948.

[2] Hashemi-Afzal, F.; Fallahi, H.; Bagheri, F.; Collins, M. N.; Eslaminejad, M. B.; Seitz, H. Advancements in hydrogel design for articular cartilage regeneration: A comprehensive review. *Bioact. Mater.* **2025**, *43*, 1-31.

[3] Chen, M.; Jiang, Z.; Zou, X.; You, X.; Cai, Z.; Huang, J. Advancements in tissue engineering for articular cartilage regeneration. *Heliyon* **2024**, *10(3)*.

[4] Wang, Z.; Hong, H.; Zhai, Z.; Yao, Y.; Zhou, T.; Zhang, H.; Gao, C. Reactive oxygen species-scavenging nanoparticles coated with chondroitin sulfate protect cartilage against osteoarthritis in vivo. *Nano Res.* **2023**, *16*(2), 2786-2797.

[5] Hu, D.; Liu, D.; Hu, Y.; Wang, Y.; Lu, Y.; Bai, C.; Wang, X. Dual-physical network PVA hydrogel commensurate with articular cartilage bearing lubrication enabled by harnessing nanoscale crystalline domains. *Nano Res.* **2024**, *17*(11), 9784-9795.

[6] Wang, Q.; Li, Y.; Chen, X.; Jiang, H.; Zhang, Z.; Sun, X. Optimized in vivo performance of acid-liable micelles for the treatment of rheumatoid arthritis by one single injection. *Nano Res.* **2019**, *12*(2), 421-428.

[7] Pellicore, M. J.; Gangi, L. R.; Murphy, L. A.; Lee, A. J.; Jacobsen, T.; Kenawy, H. M.; Hung, C. T. Toward defining the role of the synovium in mitigating normal articular cartilage wear and tear. *J. Biomech.* **2023**, *148*, 111472.

[8] Choudhari, A.; Gupta, A. K.; Kumar, A.; Kumar, A.; Gupta, A.; Chowdhury, N.; Kumar, A. Wear and friction mechanism study in knee and hip rehabilitation: A comprehensive review. *Applications of Biotribology in Biomedical Systems* **2024**, 345-432.

[9] van den Bosch, M. H.; Blom, A. B.; van den Bosch, M. H.; Blom, A. B.; van der Kraan, P. M. Inflammation in osteoarthritis: Our view on its presence and involvement in disease development over the years. *Osteoarthr. Cartilage* **2024**, *32(4)*, 355-364.

[10] Bernal-Alvarez, L. R.; Ramirez-Gutierrez, C. F.; Gomez-Vazquez, O. M.; Correa-Piña, B. A.; Zubieta-Otero, L. F.; Millán-Malo, B. M.; Rodriguez-Garcia, M. E. Enhancing surface chemistry and wetting behavior of laser-modified Ti − 6Al − 4V surgical titanium alloy surfaces through wet deposition of biogenic hydroxyapatite. *Surf. Coat. Tech.* **2024**, *489*, 131065.

[11] Marin, E.; Lanzutti, A. Biomedical applications of titanium alloys: a comprehensive review. *Materials* **2023**, *17(1)*, 114.

[12] Hijazi, K. M.; Dixon, S. J.; Armstrong, J. E.; Rizkalla, A. S. Titanium alloy implants with lattice structures for mandibular reconstruction. *Materials* **2023**, *17(1)*, 140.

[13] Lin, X.; Zhang, L.; Duan, B. Polyphenol-mediated chitin self-assembly for constructing a fully naturally resourced hydrogel with high strength and toughness. *Mater. Horiz.* **2021**, *8(9)*, 2503-2512.

[14] Hu, L.; Chee, P. L.; Sugiarto, S.; Yu, Y.; Shi, C.; Yan, R.; Huang, W. Hydrogel - based flexible electronics. *Adv. Mater.* **2023**, *35(14)*, 2205326.

[15] Li, X.; Gong, J. P. Design principles for strong and tough hydrogels. *Nat. Rev. Mater.* 9(6), **2024**, 380-398.

[16] Chen, Y.; Zhou, Y.; Hu, Z.; Lu, W.; Li, Z.; Gao, N.; He, Y.; Gelatin-based metamaterial hydrogel films with high conformality for ultra-soft tissue monitoring. *Micron -Micro Lett.* **2024**, *16(1)*, 34.

[17] Choi, S.; Moon, J. R.; Park, N.; Im, J.; Kim, Y. E.; Kim, J. H.; Kim, J. Bone - adhesive anisotropic tough hydrogel mimicking tendon enthesis. *Adv. Mater.* 35(3), **2023**, 2206207.

[18] Petelinšek, N.; Mommer, S. Tough hydrogels for load - bearing applications. *Adv. Sci.* 11(12), **2024**, 2307404.

[19] Zhang, X.; Chen, Q.; Chen, K.; Feng, H.; Feng, C.; Li, X.; Ge, S. Tough, Slippery, and Low-Permeability Multilayer Hydrogels Modified by Anisotropic Fiber Membrane for Soft Tissue Replacement. *ACS Appl. Mater. Interfaces* **2024**, *16(36)*, 47314-47324.

[20] Liu, H.; Zhao, W.; Zhang, Y.; Zhao, X.; Ma, S.; Scaraggi, M.; Zhou, F. Robust Super - Lubricity for Novel Cartilage Prototype Inspired by Scallion Leaf Architecture. *Adv. Funct. Mater.* **2024**, *34(16)*, 2310271.

[21] Gurav, A. B.; Shi, H.; Duan, M.; Pang, X.; Li, X. Highly transparent, hot water and scratch resistant, lubricant-infused slippery surfaces developed from a mechanically-weak superhydrophobic coating. *Chem. Eng. J.* **2021**, *416*, 127809.

[22] Sharma, S. K.; Pradhan, R.; Grewal, H. S. Sustainable Manufacturing of Multifunctional Fluorine-Free Superslippery Flexible Surfaces. *ACS Appl. Mater. Interfaces* **2024**, *16(33)*, 44139-44151.

[23] Zhang, Z.; Ma, Y.; Yu, B.; Ma, S.; Yang, H.; Liu, L.; Zhou, F. Vertical and Horizontal Double Gradient Design for Super - Slippery and High - Bearing Hydrogel Skeleton. *Adv. Funct. Mater.* **2024**, *34(29)*, 2400360.

[24] Chen, K.; Chen, Q.; Yan, X.; Zhang, X.; Feng, H.; Feng, C.; Ge, S. Bioinspired design of strong, tough and slippery hydrogels beyond the natural soft tissues. *Mater. Today Chem.* **2025**, *45*, 102633.

[25] Zeng, L.; Fu, Y.; Cui, H.; Zhao, Y.; Liu, Y.; Lin, X.; Guo, H. Strong, Smart, and Slippery Organo - gels by Network Glassification. *Adv. Funct. Mater.* **2024**, *34(44)*, 2407397.

[26] Chen, J.; Li, C.; Chen, X.; Zhou, K.; Li, H.; Peng, K.; Huang, B. In situ swelling of low-friction, high load-bearing self-bending bilayer hydrogels inspired by articular cartilage. *Biomed. Mater.* **2025**, *20(2)*, 025018.

[27] Wang, Y.; Li, H.; Li, J.; Zhang, W.; Wu, C. Porous PVA - PAM - AG Multi - Network Hydrogel With High Mechanical Strength. *J. Appl. Polym. Sci.* 142(18), **2025,** e56836.

[28] Jiang, X.; Sun, Y.; Lyu, Y.; Kang, H.; Zhao, J.; Zhang, K.; Bian, L. Hydrogels for ameliorating osteoarthritis: mechanical modulation, anti - inflammation, and regeneration. *BMEMat* **2024**, *2(2)*, e12078.

[29] Dufrêne, Y. F.; Viljoen, A.; Mignolet, J.; Mathelié - Guinlet, M. AFM in cellular and molecular microbiology. Cell. *Microbiol.* **2021**, *23(7)*, e13324.

[30] Schwartz, J. J.; Jakob, D. S.; Centrone, A. A guide to micron scale IR spectroscopy: resonance enhanced transduction in contact and tap mode AFM-IR. *Chem. Soc. Rev.* **2022**, *51(13)*, 5248-5267.

[31] Heath, G. R.; Kots, E.; Robertson, J. L.; Lansky, S.; Khelashvili, G.; Weinstein, H.; Scheuring, S. Localization atomic force microscopy. *Nature* **2021**, *594(7863)*, 385-390.

[32] Zhang, H.; Wang, Y.; Yu, T.; Liu, Z. Microstructural characteristics of differently aged asphalt samples based on atomic force microscopy (AFM). *Constr. Build. Mater.* **2020**, *255*, 119388.

[33] Li, Y.; Yang, J.; Pan, Z.; Tong, W. Micron scale pore structure and mechanical property analysis of coal: An insight combining AFM and SEM images. *Fuel* **2020**, *260*, 116352.

[34] Isaacs, M. A.; Davies-Jones, J.; Davies, P. R.; Guan, S.; Lee, R.; Morgan, D. J.; Palgrave, R. Advanced XPS characterization: XPS-based multi-technique analyses for comprehensive understanding of functional materials. *Mater. Chem. Front.* **2021**, *5(22)*, 7931-7963.

[35] Chen, X.; Wang, X.; Fang, D. A review on C1s XPS-spectra for some kinds of carbon materials. *Fuller. Micron tub. Car. N.* **2020**, *28(12)*, 1048-1058.

[36] Krishna, D. N. G.; Philip, J. Review on surface-characterization applications of X-ray photoelectron spectroscopy (XPS): Recent developments and challenges. *Applied Surface Science Advances* **2022**, *12*, 100332.

[37] Tougaard, S. Practical guide to the use of backgrounds in quantitative XPS. *J. Vac. Sci. Technol. A* **2021,** *39(1)*.

[38] Shard, A. G. Practical guides for x-ray photoelectron spectroscopy: Quantitative XPS. *J. Vac. Sci. Technol. A* **2020**, *38(4)*.

Electronic Supplementary Material

Super-lubricating hydrogel enabled by microgel rolling and gradient porous structures

Song Yang[1, 2], Chenxi Qin[2], Zhencai Xing[3], Ming Zhang[2,*], Yanfei Ma[2,*] Feng Zhou[2], and Weimin Liu[1, 2, *]

[1] *School of Materials Science and Engineering, Northwestern Polytechnical University, Xi'an 710072, China*
[2] *State Key Laboratory of Solid Lubrication, Lanzhou Institute of Chemical Physics, Chinese Academy of Sciences, Lanzhou 730000, China*
[3] *Shandong Laboratory of Yantai Advanced Materials and Green Manufacture, Yantai 264006, China*
**Corresponding author. E-mail: mayanfei@licp.cas.cn, zhm@licp.cas.cn, wmliu@licp.cas.cn*

Supporting information to https://fo.org/10.26599/NR.2026.94908384

Address correspondence to Ming Zhang, zhm@licp.cas.cn; Yanfei Ma, mayanfei@licp.cas.cn; Weimin Liu, wmliu@licp.cas.cn

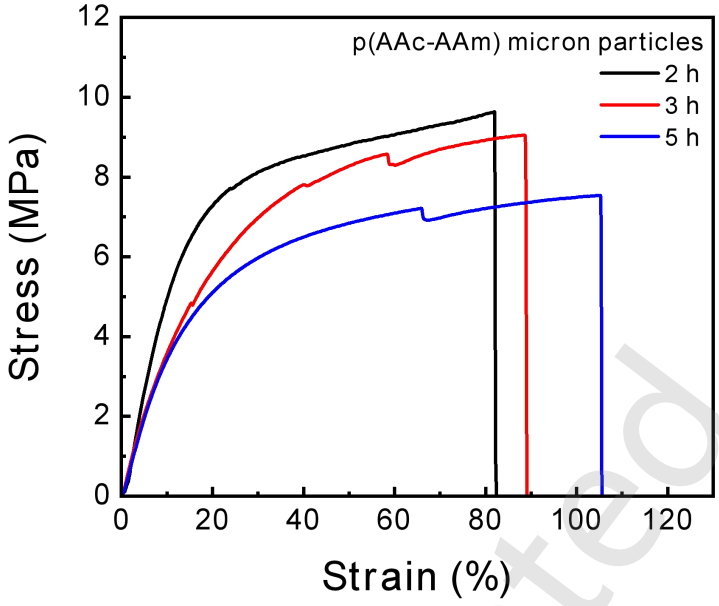

Fig. S1 The tensile stress-strain curves of hydrogels with nanoparticles added after 2 hours, 3 hours and 5 hours of UV irradiation.

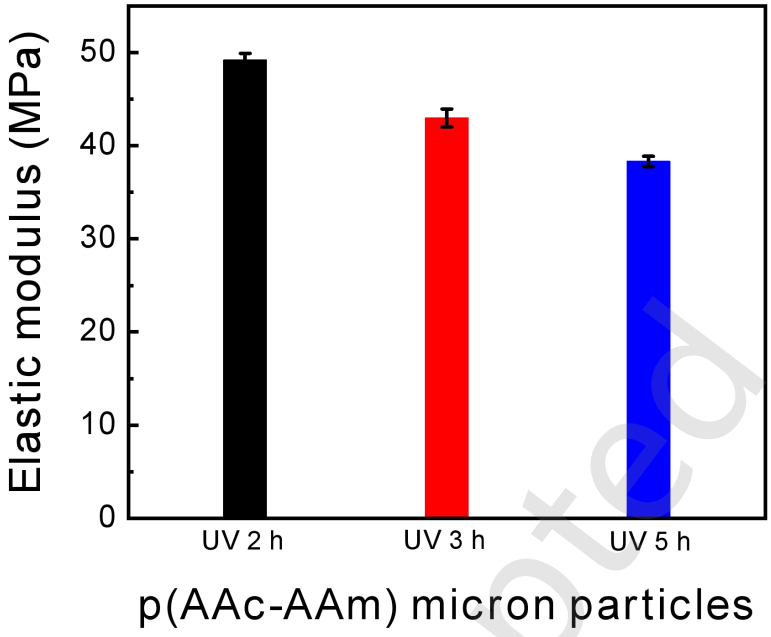

Fig. S2 The elastic modulus of hydrogels with nanoparticles added after 2 hours, 3 hours and 5 hours of UV irradiation.

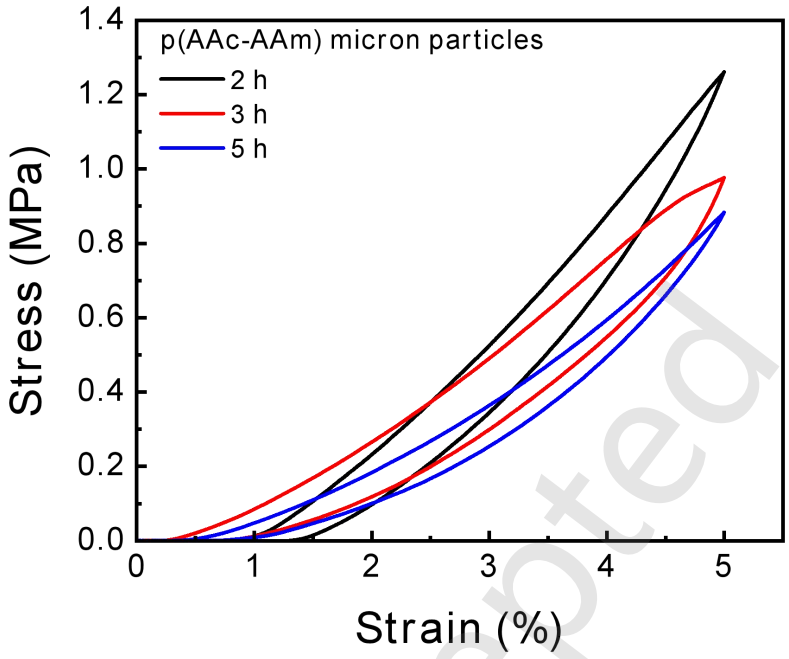

Fig. S3 The compressibility of hydrogels with nanoparticles added after 2 hours, 3 hours and 5 hours of UV irradiation.

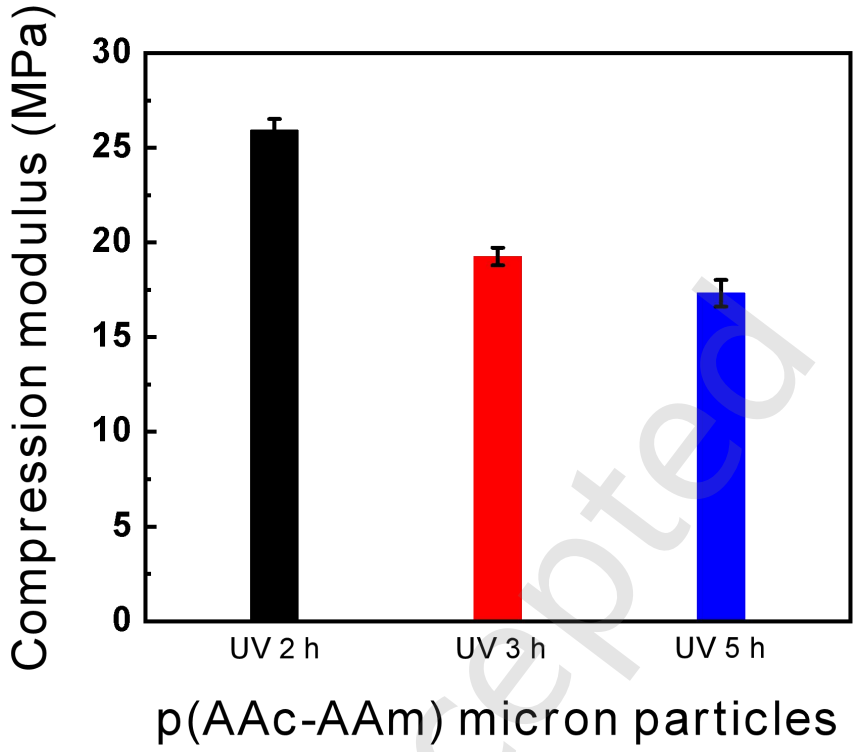

Fig. S4 The compression modulus of hydrogels with nanoparticles added after 2 hours, 3 hours and 5 hours of UV irradiation.

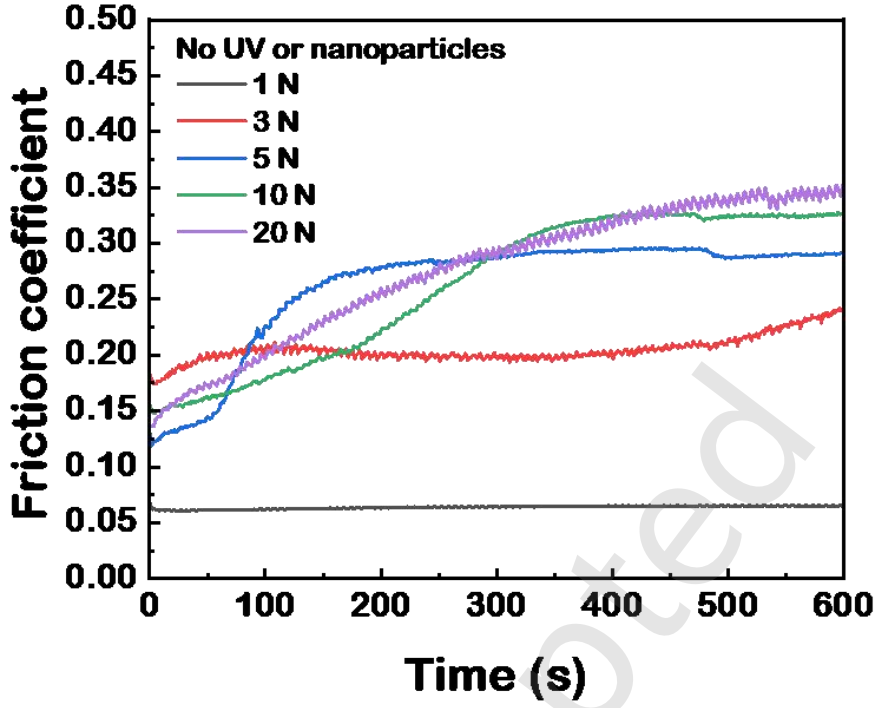

Fig. S5 Friction of hydrogel without nano particles and UV light.

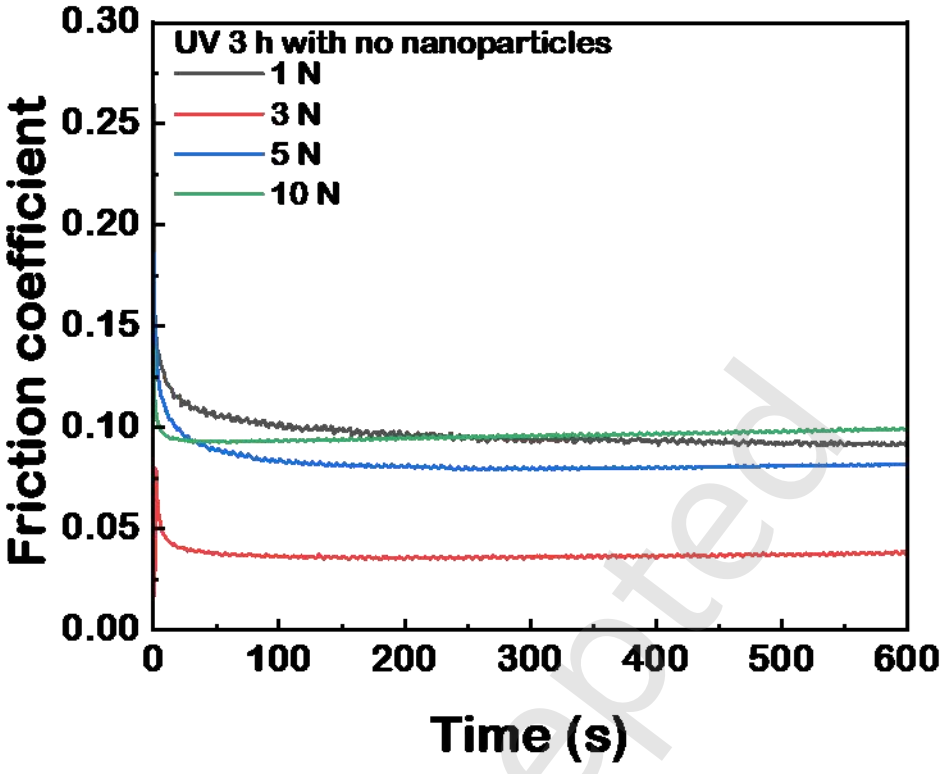

Fig. S6 Friction performance of UV light without adding nanoparticles for 3 hours.